Journal of Alloys and Compounds 698 (2017) 906–912

Contents lists available at ScienceDirect

Journal of Alloys and Compounds

journal homepage: http://www.elsevier.com/locate/jalcom

Grain and interface boundaries governed strengthening mechanisms in metallic multilayers

Qing Zhou [a], Ping Huang [a, **], Mabao Liu [b], Fei Wang [b, c, *], Kewei Xu [a], Tianjian Lu [b, c]

[a] State Key Laboratory for Mechanical Behavior of Material, School of Materials Science and Engineering, Xi'an Jiaotong University, Xi'an 710049, China
[b] State Key Laboratory for Strength and Vibration of Mechanical Structures, School of Aerospace, Xi'an Jiaotong University, Xi'an 710049, China
[c] MOE Key Laboratory for Multifunctional Materials and Structures, School of Aerospace, Xi'an Jiaotong University, Xi'an 710049, China

ARTICLE INFO

Article history:
Received 5 October 2016
Received in revised form
2 December 2016
Accepted 19 December 2016
Available online 24 December 2016

Keywords:
Multilayer
Nanoindentation
Hardness
Interface
Grain boundary

ABSTRACT

To tailor the mechanical properties of an engineering material, manipulating its internal boundaries such as grain/interface boundaries (GBs/IBs) is a standard practice. Upon reevaluating the hardness of Cu/Al, Cu/W and other bimetallic multilayer systems, we demonstrated that apart from IBs, GBs also contribute to the strengthening process of polycrystalline multilayers. By analyzing in detail the coupling and competing effects between IBs and GBs, we revealed experimentally that the strength contributed from incoherent IBs in *face-centered cubic/body-centered cubic* (fcc/bcc) multilayer systems is lower than that from bcc GBs and fcc/fcc IBs. In light of existing data and theory, interface shear was proposed as the main mechanism, providing reasonable explanation of the "weakening effects" of incoherent IBs.

1. Introduction

Nanoscale metallic multilayers have attracted scientific and practical interest on their significantly elevated mechanical strength [1–7]. Nanoindentation is often used to evaluate the hardness and Young's modulus of multilayer materials [8], which is proved to be a powerful tool in delineating the mechanical properties of thin film composites with different combinations. The yield strength of certain metallic multilayers, about 1/3 of nanoindentation hardness, could approach 1/2 to 1/3 of theoretical strength limit (i.e., $E/30$, E being Young's modulus) as the layer thickness (h) was decreased from micrometer to nanometer [5]. Further, numerous studies demonstrated that the peak hardness (H_{max}) of a multilayer with two constituent layers was larger than the hardness (H_{rom}) derived by the rule of mixture (ROM) theory of averaging the hardness of its monolithic layers, as shown in Fig. 1 (black rectangle), Tables 1 and 2. Such astonishing results were intimately tied to high density heterogeneous interface boundaries (IBs) between dissimilar constituent layers and not the crystals they join.

However, the role of IBs in multilayers was often treated in a phenomenological way as grain boundaries (GBs) in nanocrystalline materials, leading to scaling laws that related strength to the spacing between adjacent interface barriers. For epitaxial multilayers, the only microstructural scale of significance was h, as models based on interface theory largely obscured the polycrystalline nature of the constituent layers. The in-plane grain size (d) was often found to scale with h [4,7]. Once the peak hardness was obtained for multilayers with reduced h, GBs perpendicular to IBs should inevitably contribute to the strengthening process of polycrystalline multilayers [7–10]. In other words, the constraints of both GBs and IBs to gilding dislocations acted concurrently to enhance the peak hardness [8]. Thus, strengthening mechanisms related to the two characterizing length scales (i.e., h and d) should overlap and hence could rarely be separated. So far, however, little effort had been devoted to probing the separate contributions of IBs and GBs to hardness (strength) enhancement of a multilayer. The relationship between hardness enhancement and IB structures needs more consideration from the perspective of GBs as a

* Corresponding author. State Key Laboratory for Strength and Vibration of Mechanical Structures, School of Aerospace, Xi'an Jiaotong University, Xi'an 710049, China.
** Corresponding author.
E-mail addresses: huangping@mail.xjtu.edu.cn (P. Huang), wangfei@mail.xjtu.edu.cn (F. Wang).

http://dx.doi.org/10.1016/j.jallcom.2016.12.254
0925-8388/

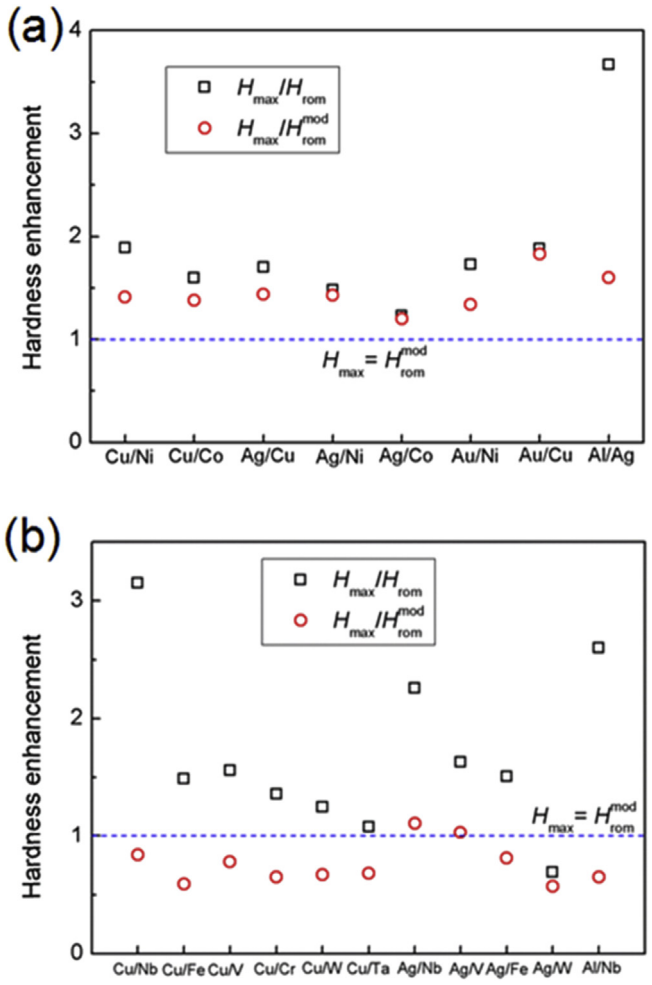

Fig. 1. Hardness enhancement H_{max}/H_{rom} and back-calculated H_{max}/H_{rom}^{mod} in (a) fcc/fcc (hcp) and (b) fcc/bcc multilayers.

Table 1
Hardness enhancement H_{max}/H_{rom} in fcc/fcc (hcp) multilayers.

Systems	Peak hardness (GPa)	Elasticity mismatch	H_{max}/H_{rom}	References
Cu/Ni	6.83	1.65	1.89	[43]
Cu/Nb	7.78	1.11	1.99	[28]
Cu/Co	6.00	1.75	1.60	[17]
Ag/Cu	4.60	1.48	1.70	[4]
Ag/Ni	6.20	1.60	1.48	[44]
Ag/Co	4.90	1.90	1.23	[18]
Au/Cu	2.45	1.79	1.88	[33]
Au/Ni	6.50	2.81	1.73	[45]
Al/Ag	5.50	1.15	3.67	[1]

Table 2
Hardness enhancement H_{max}/H_{rom} in fcc/bcc multilayers.

Systems	Peak hardness (GPa)	Elasticity mismatch	H_{max}/H_{rom}	References
Cu/Nb	7.02	1.11	3.15	[34]
Cu/Fe	4.80	1.61	1.49	[46]
Cu/V	5.20	1.03	1.56	[23]
Cu/Cr	6.80	2.40	1.36	[47]
Cu/W	8.90	3.30	1.25	[48]
Cu/Ta	7.00	1.44	1.08	[10]
Ag/Nb	7.90	1.25	2.26	[16]
Ag/V	5.70	1.55	1.63	[49]
Ag/Fe	6.36	2.20	1.51	[50]
Ag/W	6.9	3.79	0.69	[51]
Al/Nb	4.80	1.44	2.60	[23]

strengthen source.

In this paper, the hardness of Cu/Al and Cu/W multilayers were compared to that of single-component nanocrystalline materials with same grain size. Additionally, upon processing experimental hardness data from the open literature, we presented results concerning the competition and synergism of GBs and IBs to the overall hardness of metallic multilayers. Upon removing the separated contribution of GBs, we provided an understanding of interface-structure-dependent strengthening mechanisms in metallic multilayers.

2. Experimental procedures

A series of Cu/Al and Cu/W multilayers with equal individual thickness h ranging from 5 to 200 nm were deposited on Si (100) at room temperature by magnetron sputtering. The total thickness of each multilayer specimen was fixed at ~2.0 μm. The cross-sectional microstructures of each multilayer were evaluated by high resolution transmission electron microscopy (HRTEM) analysis via JEOL-2100F operating at 200 kV.

The mechanical properties of as-deposited multilayers were evaluated by nanoindentation testing via a dynamic contact module device equipped with the Nanoindenter XP system (MTS, Inc.). Upon calibration with standard fused silica, the three-sided pyramid Berkovich diamond indenter was penetrated into the top of the films under continuous stiffness measurement (CSM) mode. The Nanoindenter XP system provides an allowable-drift-rate at 0.005 nm s^{-1} to set the thermal stability criterion for initiating the testing, which is 10-fold smaller than the default value 0.05 s^{-1} generally used in hardness tests. The maximum indentation depth is fixed at 300 nm for each multilayer at room temperature using the depth control mode, and the intrinsic hardness was calculated by averaging hardness data obtained within a certain depth range (10–15% of total thickness). At least 16 indentations were conducted for each multilayer sample.

3. Results

The TEM graph of Cu/Al multilayer with $h = 100$ nm exhibited clear modulation structures with epitaxial relationship of fcc Cu (111)//Al (111), as shown in Fig. 2a. Cu/W multilayer with $h = 10$ nm showed epitaxial relationship of fcc Cu (111)//bcc W (110). Distinguished IBs and GBs are visible, with grain size d approximately equal to layer thickness h, as seen in Fig. 2b and c.

Indentation hardness values for Cu/Al and Cu/W were plotted as a function of h in Fig. 3. For Cu/Al films, the hardness increased monotonically as h was decreased from 200 to 5 nm, and the smallest length scale controlled the peak hardness (5.9 GPa). In Cu/W, the peak hardness of 9.8 GPa developed at 10 nm layer thickness. For comparison, the hardness of nanocrystalline single-layer Cu, Al and W films (all 2 μm thick) was measured to be 2.1 GPa, 1.1 GPa and 16.2 GPa, respectively. The maximum hardness achieved in the present multilayers was significantly higher than the rule of mixture (ROM) estimation (dotted lines in Fig. 3), suggesting the interface strengthening effect. However, while the hardness data of Cu/Al all lied above the ROM line, those of Cu/W did not. A direct comparison between H_{max} and H_{rom} was unreasonable, as the effects of GBs on hardness needed to be considered first.

As the grain size in individual layers would reduce when the layer thickness dropped to nanometer scale [4,7], GB strengthening in multilayers would operate remarkably in the same way as the classical Hall-Petch (H–P) relation for a polycrystalline film. For GB strengthening, the GBs acted as pinning points to impede further dislocation propagation [11,12]. As d fell into the nano-regime, the hardness varied as [12]:

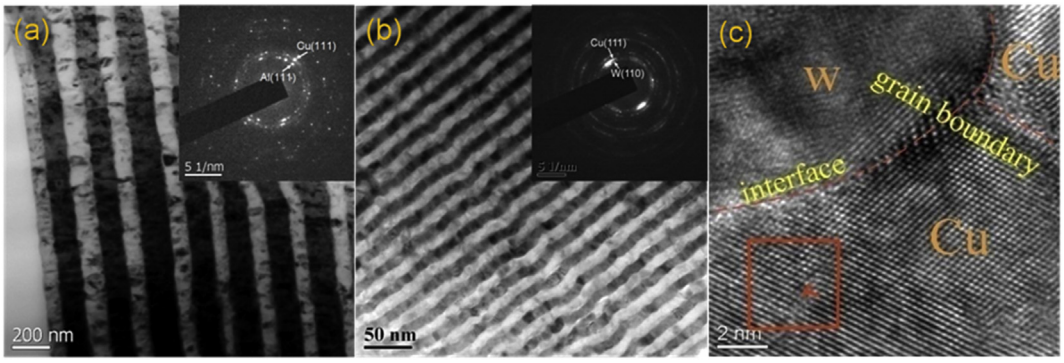

Fig. 2. Representative TEM images of (a) Cu 100 nm/Al 100 nm, (b) Cu 10 nm/W 10 nm. (c) HRTEM images of Cu 10 nm/W 10 nm.

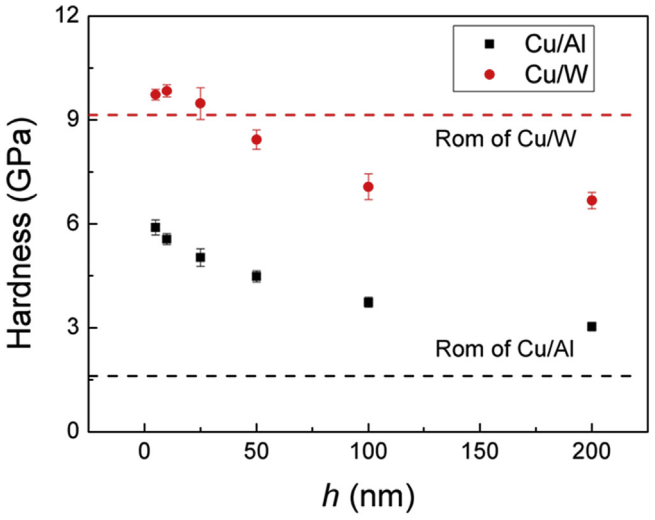

Fig. 3. Hardness of Cu/Al and Cu/W plotted as a function *h*.

$$H = H_0 + kd^{-1/2}, d \geq d_c \tag{1a}$$

$$and\ H = H_0 + kd_c^{-1/2}, d \leq d_c \tag{1b}$$

where H_0 is the intrinsic hardness of coarse-grained sample, k is the Hall-Petch coefficient (Table 3), and d_c (about 20 nm for general case) is critical grain size below which H–P relation breaks down [12]. Accordingly, at such small length scale, the modified rule-of-mixtures hardness (H_{rom}^{mod}) for a multilayer with two constituent phases of A and B could be defined as [13]:

Table 3
Hall–Petch coefficient k for polycrystalline elements involved in Tables 1 and 2.

Elements	μ (GPa)	a_0 (nm)	b (nm)	k (GPa × nm$^{1/2}$)	References
fcc Cu	48	0.362	0.255	10.0	[52]
fcc Ag	30	0.409	0.289	4.2	[53]
fcc Ni	76	0.352	0.248	9.9	[54]
fcc Au	27	0.408	0.289	7.9	[55]
fcc Al	26	0.404	0.286	9.0	[56]
hcp Co	81	0.353	0.251	10.9	[57]
bcc Nb	37.5	0.33	0.286	33.2	[58]
bcc Fe	82	0.287	0.248	22.1	[59]
bcc V	46.4	0.303	0.263	30.0	[60]
bcc Cr	115	0.29	0.250	43.6	[35]
bcc W	131	0.317	0.274	183.5	[61]

$$H_{rom}^{mod} = f_A H_A + f_B H_B = f_A(H_0^A + k_A {d_A}^{-1/2}) + f_B(H_0^B + k_B {d_B}^{-1/2}) \tag{2}$$

where f is the volume fraction of constituent layers and d is the grain size inside individual layer, which is generally considered to be identical to h when maximum hardness of the multilayer is achieved [4,7].

Based on Eq. (2), H_{rom}^{mod} of Cu/Al was calculated as 3.2 GPa, which was lower than $H_{\max}$ of Cu 5 nm/Al 5 nm, while H_{rom}^{mod} of 13.1 GPa for Cu/W was obviously higher than $H_{\max}$ of Cu 10 nm/W 10 nm. For further comparison, the hardness enhancement in other multilayers reported previously in Fig. 1 was recalculated as H_{max}/H_{rom}^{mod}. The results shown as red circle revealed that face-centered cubic (fcc)/fcc and fcc/hexagonal close-packed (hcp) multilayers exhibited comparable hardness when corresponding NC metals were confined at identical length scales. Moreover, obvious weakening effects (e.g., $H_{max}/H_{rom}^{mod}<1$) had been found in numerous fcc/bcc multilayer systems, except for Ag/V and Ag/Nb multilayers, as shown in Fig. 1b. For Ag/V multilayers, continuous bcc–fcc phase transformation was observed through the Bain orientation [14], where the formation of coherent IBs took place. The unusual behavior Ag/Nb multilayer was originated from a unique amorphous microstructure formed at the IBs [15], which was beyond the scope of this study. So, given that the interface contribution decreased from coherent/semi-coherent IBs in fcc/fcc multilayers (including fcc/hcp due to phase transformation [16,17] from hcp to fcc when h is small) to incoherent IBs in fcc/bcc multilayers, hardness contribution from IBs should be further quantified.

For nanocrystalline materials, the mixture model proposed by Kim et al. [18] is one common approach to explain the deformation mechanism. Follow that thinking, here we consider a multilayer material consisting of GBs and IBs. When h is dropped below tens of nanometers, the average in-plane grain size is approximately equal to the layer thickness [4,7]. As a result, the chances for a dislocation to be blocked by either GBs or IBs might be same, so that the hardness contributed from grain refinement could be reasonably taken as one half of H_{rom}^{mod} in Eq. (2). Accordingly, the hardness contribution from interface barrier, H_{int}, may be obtained as:

$$H_{int} = H_{mul} - \frac{1}{2}H_{rom}^{mod} \tag{3}$$

The hardness contribution from IBs calculated from Eq. (3) was presented in Fig. 4. Clearly, most of the enhanced hardness of coherent/semi-coherent IBs (black dots) was larger than that of incoherent IBs (red dots). In view of the results of Fig. 4, we presented a discussion of interface structure dependent strengthening

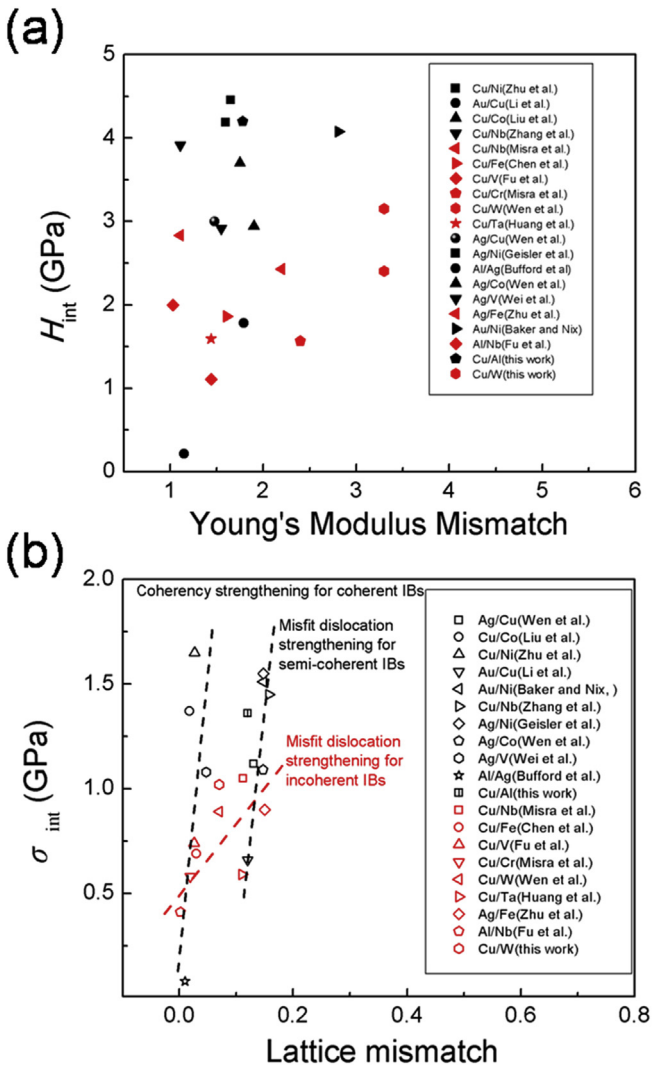

Fig. 4. (a) Correlation between hardness contribution from IB barrier and modulus mismatch between constituent elements in multilayers. Black symbols indicated fcc/fcc multilayers with coherent/semi-coherent IBs and red symbols indicated fcc/bcc multilayers with incoherent IBs. (b) Interface barrier strength plotted as a function of lattice mismatch. Black symbols indicated multilayers with coherent/semi-coherent IBs and red symbols indicated multilayers with incoherent IBs. (For interpretation of the references to colour in this figure legend, the reader is referred to the web version of this article.)

mechanism in the following section.

4. Discussion

Previously, it had been postulated that the Peach Koehler plays an important role in interface strengthening in multilayers, especially those having large elastic modulus mismatch [19]. The model that modulus mismatch induced enhanced hardness was further developed by Lehoczky [20,21]. The yield stress $\sigma_{\max}$ for a multilayer with equal layer thickness of phases A and B could be obtained as [17]:

$$\sigma_{\max} = \frac{1}{2}\left(1+\frac{E_B}{E_A}\right)\left(\sigma_m + \sigma_m^A\right) \quad (4)$$

where σ_m^A is equivalent to the yield strength of as-deposited monolayer A, and σ_m is the strength contribution from IBs.

It is clear from Eq. (4) that a larger modulus mismatch (E_B/E_A) between constituent layers may cause higher strength/hardness [22]. However, the results shown in Fig. 4a demonstrated that the hardness did not increase with modulus mismatch as expected. This implied that other interface dependent mechanism(s) may operate simultaneously, which are likely to depend upon atomic structure of IBs.

4.1. Fcc/fcc multilayers with coherent/semi-coherent IBs

For a fcc/fcc multilayer with identical crystal structures and slip systems in both constituent layers, the significantly enhanced hardness was attributed to elastic mismatch and lattice mismatch pre-existing in the multilayer [23–25]. Therefore, the lattice parameter in constituent layers also played a crucial role in influencing the hardness. For small lattice mismatch (δ <0.1 [26]), coherency was achieved in multilayers when h is below an acritical value, such as Cu/Ni, Cu/Co, Ag/Al. Otherwise, larger lattice mismatches could effectively lead to misfit dislocations at interfaces in multilayers such as Cu/Al, Ag/Cu, Au/Cu, Cu/Nb (fcc/fcc [27]), Ag/Ni, and Ag/Co.

According to the coherent stress model, alternating compressive and tensile in-plane stresses could inhibit dislocation movement, resulting in enhanced strength/hardness of multilayers [28]. Macro-yielding was expected when the applied stress was sufficiently to eliminate stresses with alternating signs [29] and the maximum strength enhancement was given by Refs. [28–31]:

$$\sigma_{coh} = m\cdot(1/6)^{1/2}AE\delta\cdot\left(\frac{h_c}{h}\right) \quad (5)$$

where $A = 0.5$ is the composition modulation amplitude for a multilayer, E is the average elastic modulus, and h_c is the critical layer thickness for coherency, below which the multilayer is assumed to have maximum coherent stress [30].

In multilayers having large lattice mismatch, the misfit may be too large to achieve coherency and misfit dislocations would be introduced. Hoagland et al. [23] employed atomic simulations to examine slip behavior in coherent and semi-coherent metallic bi-layered composites, and concluded that semi-coherent IBs could act as barriers to slip due to interaction between misfit and glide dislocations. Upon summarizing experiment results for a large number of multilayer systems, Li et al. [32] found that interface strengthening effect increased with the increasing lattice mismatch. It was further demonstrated that misfit dislocation network played an important role in affecting interface strengthening behavior as [32]:

$$\sigma_d = m\cdot\alpha\cdot\mu^*\sqrt{\frac{2b(\delta-\varepsilon)}{h}} \quad (6)$$

where α (~0.3) is a material constant, and $\varepsilon = 0.76\delta$ [32] is the residual elastic strain parallel to interface plane.

Based on the aforementioned studies, Fig. 4b showed that the interface resistance as a function of lattice mismatch (black dashed line for fcc/fcc). However, while there was a trend that hardness increases with lattice mismatch, significant deviations also existed. For example, Cu/Ag and Ag/Co had similar IBs resistance despite that a large difference existed in their lattice mismatch. Thus, it was clear that the contribution to strength/hardness from IBs could not be interpreted solely based on lattice mismatch.

More precisely, to reveal the interface-dependent strengthening mechanism, the interface barrier strength σ_{int} could be specified as:

$$\sigma_{int} = \sigma_k + \sigma_{coh} + \sigma_d + \sigma_{ch} + \sigma_f \quad (7)$$

where σ_k is the Koehler stress originating from modulus mismatch, σ_{coh} is derived from coherency stress, σ_d is determined by misfit dislocations at IBs, σ_{ch} is the chemical interaction term related to stacking fault energy (SFE) difference between constituent layers, and σ_f is the interface stress.

The first term, σ_k, predicted that a large stress is required to drive dislocation across IBs from a layer with lower elastic modulus into the one with higher modulus [1]:

$$\sigma_k = \frac{m\mu_A(\mu_B - \mu_A)b\sin(\theta)}{4\pi(\mu_B + \mu_A)h} \quad (8)$$

where θ is the angle between the interface and the glide planes.

The chemical mismatch term σ_{ch} arising from SFE difference in A/B multilayers may be approximated as [29]:

$$\sigma_{ch} = m\frac{\gamma_B - \gamma_A}{b} \quad (9)$$

where γ is the SFE of the constituent layers.

The characteristic interface stress σ_f due to elastic deformation of the interfacial region may be expressed as [33]:

$$\sigma_f = \frac{f}{h} \quad (10)$$

where f (1–3 J/m^2) is the interface energy. The stress is negative under compression for hardness testing [33].

Based on Eqs. (7)–(10), the calculated values of σ_k, σ_{coh}, σ_d, σ_{ch} and σ_f for Cu/Al were summarized in Table 4. As a result, σ_{int} was estimated to be 1.44 GPa, which was comparable to the strength (H_{int}/2.7) of 1.42 GPa deduced from Eq. (3). In addition to Cu/Al, Table 4 also listed σ_{int} estimated for other fcc/fcc multilayer systems. The results of Table 4 showed clearly that the IB resistance from lattice mismatch was more pronounced than other parameters.

Since IBs in fcc/fcc multilayers are effective strengtheners, GBs in these systems may play a limited role. The competition between GBs and IBs may be understood by comparing the critical resolved shear stress (CRSS) needed to overcome the boundary resistance. The critical shear stress required for fcc/fcc interface transmission ranged from 170 MPa to 539 MPa (σ_{int}/m calculated from Table 4), much higher than the CRSS of 56 MPa for fcc NC metals [19] (Ag/Al was an exception since nanotwins contributed significantly to the overall hardness [1]). That is, GBs provided lower barrier than fcc/fcc IBs.

Since the stress for dislocation to transmit across IB was greater than that needed for GB, upon deformation, dislocation loops bowed initially within two adjacent IBs to overcome the GBs first. As the dislocations approached the fcc/fcc IBs (Fig. 5a), they were seriously blocked. Eventually, peak hardness of the multilayer was reached once the interfacial lock was overcome. The mechanism proposed above may explain, to a certain extent, why fcc/fcc IBs supplied a higher barrier than GBs in multilayers, as shown in Fig. 1a.

4.2. Fcc/bcc multilayers with incoherent IBs

The mechanisms as discussed above were applicable only to fcc/fcc multilayers having similar lattice structures in constituent layers. For multilayers containing both bcc and fcc phases, such as Cu/W possessing discontinuity incoherent IBs, i.e., {111}⟨110⟩ in fcc Cu layers and {110} ⟨111⟩ in bcc W layers, the contribution of coherency strains to hardness should be ignored. Interface misfit dislocations were required to remove incompatibilities and/or dissimilarities between the two lattice structures, which would act as obstacles to slip transmission [33,35]. From previous analysis of fcc/fcc multilayers, σ_d arising from misfit dislocations may be expressed as a function of shear modulus and lattice mismatch. Consequently, the variation trend of σ_{int} as a function of lattice mismatch (calculated from fcc (111)/bcc (110) interface with K–S orientation) was obtained, as shown (red dashed line) in Fig. 4b. It was seen that a larger lattice mismatch led to a higher misfit dislocation density and stronger interaction between interface and gliding dislocation, causing higher interface strengthening.

In fact, the process of slip transfer across fcc/bcc IBs was more complex than that described above. The transfer of slip across a fcc/bcc interface between two different phases must, in general, involve dislocation multiplication due to discontinuity in slip systems [36]. Consequently, incoherent IBs could not be directly crossed by dislocations. However, the dislocations were trapped therein, which weakened the strength as interface shear could occur [36]. As shown Fig. 5b, when a full lattice dislocation b_1 approached the IBs (Stage_1 and 2), it would dissociate into an interfacial dislocation b_{1i} perpendicular to the IBs and a dislocation debri b_{1d} parallel to the IBs (Stage_3). Unlike the fairly mobile misfit dislocation in fcc/fcc IBs [25,26], low interfacial shear resistance along with the spreading dislocation core in fcc/bcc IBs enabled the in-plane component of dislocation b_{1d} to glide with a high mobility, and the out-of-plane component of dislocation b_{1i} climbed in the interface through absorption and emission of vacancies [36–38]. The reactions between interfacial dislocations assisted by climb could lead to annihilation of dislocations having opposite signs, e.g., b_{1i} and b_{2i} in Satge_4, causing blunting of dislocation pileup at the interface [37,38]. Thus, it was expected that interface strengthening happened in fcc/fcc IBs (Fig. 5a) could be unlocked in fcc/bcc IBs when the partial dislocation b_{1i}, b_{2i} annihilated under interface shear. At the same time, the rapid glide dislocation debris scattered in IBs accumulated more easily in fcc/bcc interfaces than that in fcc/

Table 4
Influence of interface resistance on strengthening mechanism in selected fcc/fcc multilayer systems; σ_{cal} was calculated strength from Eq. (7); and σ_{int} was measured strength from experiments.

Interface resistance (GPa)	σ_k	σ_{coh}	σ_d	σ_{ch}	σ_f	σ_{cal}	σ_{int}	References
Cu/Ni	0.31	2.0	/	1.0	−1.71	1.60	1.65	[42]
Cu/Co	0.56	2.47	/	0.22	−2.00	1.25	1.37	[16]
Cu/Nb	0.06	/	1.19	/	−0.20	1.05	1.45	[27]
Cu/Al	0.07	/	1.02	0.95	−0.60	1.44	1.42	This work
Ag/Cu	0.15	/	1.56	0.19	−0.75	1.15	1.12	[4]
Ag/Al	0.13	0.57	/	1.55	−2.00	0.25	0.08	[1]
Ag/Ni	0.15	/	1.18	1.09	−0.60	1.82	1.55	[43]
Ag/Co	0.12	/	1.53	0.02	−0.57	1.10	1.09	[17]
Ag/V	0.09	1.45	/	/	−0.50	1.04	1.08	[48]
Au/Cu	0.01	/	0.42	0.18	−0.04	0.57	0.66	[32]
Au/Ni	0.74	/	2.61	0.71	−2.50	1.56	1.51	[44]

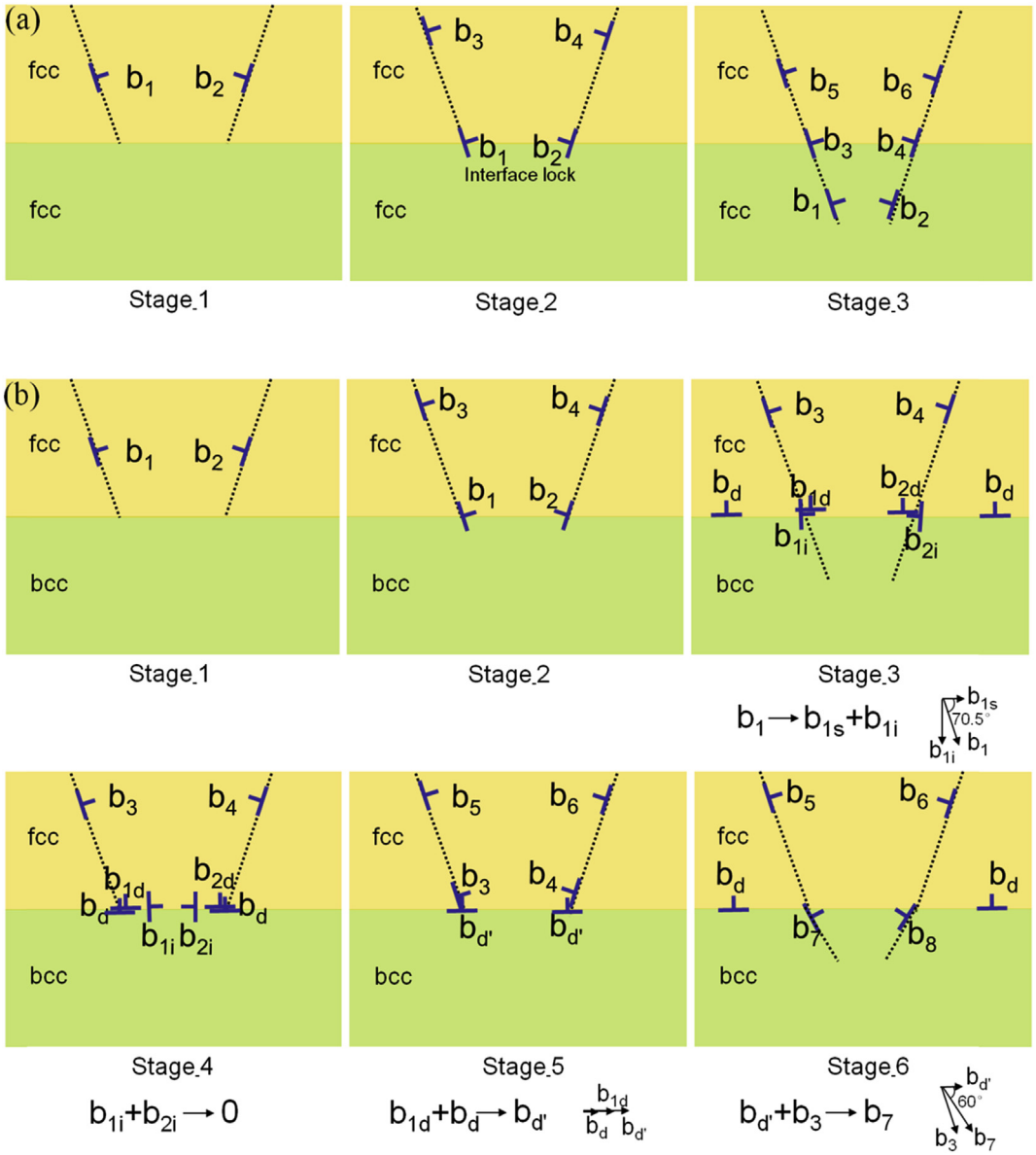

Fig. 5. (a) Schematic illustration of dislocation crossing IBs in fcc/fcc multilayers: Stage_1 dislocations approaching IBs; Stage_2 dislocations blocked by IBs; Stage_3 dislocations overcome IBs. b_1, b_2, b_3, b_4, b_5 and b_6 $1/2a_{fcc}$ (111)[110] were six lattice dislocations. Fig. 4(b) Schematic illustration of dislocation crossing IBs in fcc/bcc multilayers, with b_1, b_2, b_3, b_4, b_5 and b_6 $1/2a_{fcc}$ (111)[110] representing six lattice dislocations: Stage_1 initial configuration of two dislocations b_1 and b_2 in fcc layer approaching IBs; Stage_2 and 3 two dislocations entering the IBs were dissociated into interfacial dislocation (b_{1i}, b_{2i}) and dislocation debris (b_{1d}, b_{2d}) under interface shear; Stage_4 dislocations b_{1i} and b_{2i} climbed in interface and annihilated; Stage_5 dislocation debris b_{1d}, b_{2d} and b_d accumulated at interface under interface shear; Stage_6 lattice dislocation content b_7 and b_8 $1/2a_{bcc}$ (110)[111] in bcc layer was nucleated via combination of lattice dislocation from fcc layer (b_3 and b_4) and $b_{d'}$.

fcc interfaces, e.g., two parallel dislocations b_{1d} and b_d accumulate into $b_{d'}$ in Stage_5. This process can build up lattice dislocation content and then facilitate dislocation transmission [36] (Stage_6). Overall, in fcc/bcc multilayers, interactions between IBs and mobile dislocations to hinder successive slip would be suppressed. With the aid of dislocation slip and climb at interface, lattice dislocations were capable to overcome the IB barriers. Such IBs were likely to be incoherent that easily shear, and would not sustain the large stresses that could develop in fcc/fcc interfaces (as shown in Fig. 4).

Same as fcc/fcc multilayers, the CRSS required for fcc/bcc interface ranged from 101 MPa to 335 MPa (σ_{int}/m), lower than that of 350 MPa for bcc nanocrystalline [34]. The threshold stress for nucleating dislocations via interface shear was expected to be lower than the stress to form a dislocation from bcc GB. In other words, the ability of incoherent interface strengthening must be lower than that of bcc GB [39].

Transmission electron microscopy (TEM) studies on cold-rolled Cu/Nb multilayers showed that [40], due to the high resistance from hard phase GBs, the materials exhibited large plastic deformation without dislocation cell structure formed inside the bcc layers. Further, from in situ TEM observation of Al/Nb [38], the significantly higher dislocation density at the IBs as compared with that in Nb indicated that the dislocation mobility in Nb was lower. Since yielding in the multilayer was supposed to be realized by dislocation glide in both layers, the fcc/bcc multilayer would obtain peak strength/hardness from the high GB barriers. It is also recently noted that peak hardness is not very sensitive to the difference between two constituent elements. Still, the peak hardness is

mainly determined by the hardness from the hard constituent elements [41]. Therefore, for multilayers with incoherent IBs, enhancement in hardness from grain size refinement may be more pronounced than that derived from interface. That was the reason why a "weakening effect" had been observed in fcc/bcc multilayers ($H_{max}/H_{rom}^{mod}<1$ = in Fig. 1b).

5. Conclusion

By analyzing the competing roles of IBs and GBs in hardness enhancement, interface structure dependent strengthening mechanisms was proposed. The mechanism of lattice mismatch strengthening was postulated to play an important role in controlling the deformation in fcc/fcc multilayers, which ensured the "strengthening effect" of coherent IBs. As a result of interface shear, dislocations could effectively glide and climb at fcc/bcc IBs, which led to the "weakening effect" of incoherent IBs. This framework may be extended to aid the selection of IBs for multilayer thin film designs.

Acknowledgements

The present work was supported in part by the National Natural Science Foundation of China (51171141, 51271141, and 51471131).

References

[1] D. Bufford, Z. Bi, Q.X. Jia, H. Wang, X. Zhang, Appl. Phys. Lett. 101 (2012) 223112.
[2] Y. Zhang, T. Ouyang, D. Liu, Y. Wang, J. Du, C. Zhang, F. Feng, J. Suo, J. Alloy Compd. 666 (2016) 30–37.
[3] Q. Zhou, J.Y. Xie, F. Wang, P. Huang, K.W. Xu, T.J. Lu, Acta Mech. Sin. 31 (2015) 319.
[4] S.P. Wen, R.L. Zong, F. Zeng, Y. Gao, F. Pan, J. Mater. Res. 22 (2007) 3423.
[5] A. Misra, H. Kung, J.D. Embury, Scr. Mater. 50 (2004) 707.
[6] Q. Zhou, S. Li, P. Huang, K.W. Xu, F. Wang, T.T. Jian, Appl. Mater. 4 (2016) 096102.
[7] A. Misra, M. Verdier, H. Kung, J.D. Embury, J.P. Hirth, Scr. Mater. 41 (1999) 973.
[8] S.R. Jian, J.Y. Juang, N.C. Chen, J.S.C. Jiang, S.C. Huang, Y.S. Lai, Nanosci. Nanotech. Lett. 2 (2010) 315.
[9] Y. Zhu, Z. Li, M. Huang, J. Appl. Phys. 115 (2014) 233508.
[10] Q. Zhou, J.J. Li, F. Wang, P. Huang, K.W. Xu, T.J. Lu, Scr. Mater. 111 (2016) 123.
[11] M.X. Liu, F. Ma, P. Huang, J.M. Zhang, K.W. Xu, Mater. Sci. Eng. A 477 (2008) 295.
[12] Q. Zhou, J. Zhao, J.Y. Xie, F. Wang, P. Huang, T.J. Lu, K.W. Xu, Mater. Sci. Eng. A 608 (2014) 184.
[13] J.R. Trelewicz, C.A. Schuh, Acta Mater. 55 (2007) 5948.
[14] J.Y. Zhang, X. Zhang, R.H. Wang, S.Y. Lei, P. Zhang, J.J. Niu, J. Sun, Acta Mater. 59 (2011) 7368.
[15] Q.M. Wei, X.Y. Liu, A. Misra, Appl. Phys. Lett. 98 (2011) 11907.
[16] W.S. Lai, M.J. Yang, Appl. Phys. Lett. 90 (2007) 181917.
[17] Y. Liu, Y. Chen, K.Y. Yu, H. Wang, J. Chen, X. Zhang, Inter. J. Plast. 49 (2013) 152.
[18] S.P. Wen, F. Zeng, Y. Gao, F. Pan, Sur. Coat. Tech. 201 (2006) 1262.
[19] H.S. Kim, Y. Estrin, M.B. Bush, Acta Mater. 48 (2000) 493.
[20] J.S. Koehler, Phys. Rev. B 2 (1970) 547.
[21] S.L. Lehoczky, Phys. Rev. Lett. 41 (1978) 1814.
[22] S.L. Lehoczky, J. Appl. Phys. 49 (1978) 5479.
[23] E.G. Fu, N. Li, A. Misra, R.G. Hoagland, H. Wang, X. Zhang, Mater. Sci. Eng. A 493 (2008) 283.
[24] R.G. Hoagland, T.E. Mitchell, J.P. Hirth, H. Kung, Philo. Mag. A 82 (2002) 643–664.
[25] A. Misra, H. Krug, Adv. Eng. Mater. 3 (2001) 217.
[26] J. McKeown, A. Misra, H. Kung, R.G. Hoagland, M. Nastasi, Scr. Mater. 46 (2002) 593.
[27] R.G. Hoagland, R.J. Kurtz, V. Henager, Scr. Mater. 50 (2004) 775.
[28] J.Y. Zhang, P. Zhang, X. Zhang, R.H. Wang, G. Liu, G.J. Zhang, J. Sun, Mater. Sci. Eng. A 545 (2012) 118.
[29] J. Xu, M. Kamiko, H. Sawada, Y. Zhou, R. Yamamoto, L. Yu, I. Kojima, J. Vac. Sci. Tech. B 21 (2003) 2584.
[30] S.I. Rao, P.M. Hazzledine, Philo. Mag. A 80 (2000) 2011.
[31] A. Misra, J.P. Hirth, H. Kung, Philo. Mag. A 82 (2002) 2935.
[32] X. Chu, S.A. Barnett, J. Appl. Phys. 77 (1995) 4403.
[33] Y.P. Li, G.P. Zhang, W. Wang, J. Tan, S.J. Zhu, Scr. Mater. 57 (2007) 117.
[34] A. Misra, J.P. Hirth, R.G. Hoagland, Acta Mater. 53 (2005) 4817.
[35] D. Wu, J. Zhang, J.C. Huang, H. Bei, T.G. Nieh, Scr. Mater. 68 (2013) 118.
[36] F. Akasheh, H.M. Zbib, J.P. Hirth, R.G. Hoagland, A. Misra, J. Appl. Phys. 102 (2007) 034314.
[37] J. Wang, A. Misra, Curr. Opin. Solid State Mater. Sci. 15 (2011) 20.
[38] J. Wang, R.G. Hoagland, A. Misra, Appl. Phys. Lett. 94 (2009) 131910.
[39] N. Li, J. Wang, J.Y. Huang, A. Misra, X. Zhang, Scr. Mater. 63 (2010) 363.
[40] J.W. Yan, G.P. Zhang, X.F. Zhu, H.S. Liu, C. Yan, Philo. Mag. 93 (2013) 434.
[41] A. Misra, X. Zhang, D. Hammon, R.G. Hoagland, Acta Mater. 53 (2005) 221.
[42] Y. Kong, L. Shen, Y. Shen, Z. Chen, Mater. Sci. Eng. A 663 (2016) 29.
[43] X.Y. Zhu, X.J. Liu, R.L. Zong, F. Zeng, F. Pan, Mater. Sci. Eng. A 527 (2010) 1243.
[44] H. Geisler, K.O. Schweitz, J. Chevallier, Philo. Mag. A 79 (1999) 485.
[45] S.P. Baker, W.D. Nix, J. Mater. Res. 9 (1994) 3131.
[46] Y. Chen, Y. Liu, C. Sun, K.Y. Yu, M. Song, H. Wang, X. Zhang, Acta Mater. 60 (2012) 6312.
[47] A. Misra, M. Verdier, Y.C. Lu, H. Kung, T.E. Mitchell, M. Nastasi, J.D. Embury, Scr. Mater. 39 (1998) 555.
[48] S.P. Wen, R.L. Zong, F. Zeng, Y. Gao, F. Pan, Acta Mater. 55 (2007) 345.
[49] Q.M. Wei, N. Li, N. Mara, M. Nastasi, A. Misra, Acta Mater. 59 (2011) 6331.
[50] X.Y. Zhu, X.J. Liu, F. Zeng, F. Pan, Tran. Nonferr. Met. Soc. 20 (2010) 110.
[51] Q. Zhou, F. Wang, P. Huang, K.W. Xu, Thin Solid Films 571 (2014) 253.
[52] J. Chen, L. Lu, K. Lu, Scr. Mater. 54 (2006) 1913.
[53] X.Y. Qin, X.J. Wu, L.D. Zhang, Nanostru. Mater. 5 (1995) 101.
[54] F. Dallatorre, P. Spätig, R. Schäublin, M. Victoria, Acta Mater. 53 (2005) 2337.
[55] Y.H. Chew, C.C. Wong, F. Wulff, F.C. Lim, H.M. Goh, Thin Solid Films 516 (2008) 5376.
[56] A.S. Khan, B. Farrokh, L. Takacs, Mater. Sci. Eng. A 489 (2008) 77.
[57] A.A. Karimpoor, U. Erb, K.T. Aust, G. Palumbo, Scr. Mater. 49 (2003) 651.
[58] A.M. Omar, A.R. Entwisle, Mater. Sci. Eng. 5 (1970) 263.
[59] D. Jia, K.T. Ramesh, E. Ma, Acta Mater. 51 (2003) 3495.
[60] A.F. Jankowski, J.P. Hayes, C.K. Saw, Philos. Mag. 87 (2007) 2323.
[61] H.L. Sun, Z.X. Song, D.G. Guo, F. Ma, K.W. Xu, J. Mater. Sci. Tech. 26 (2010) 87.